Asociación Argentina
de Mecánica Computacional

Mecánica Computacional Vol XXIX, págs. 8073-8085 (artículo completo)
Eduardo Dvorkin, Marcela Goldschmit, Mario Storti (Eds.)
Buenos Aires, Argentina, 15-18 Noviembre 2010

DYNAMICS OF COHERENT STRUCTURES AND SEDIMENT TRANSPORT IN HIGH-REYNOLDS NUMBER TURBULENT FLOWS

Cristian Escauriaza

Departamento de Ingeniería Hidráulica y Ambiental, Escuela de Ingeniería, Pontificia Universidad Católica de Chile, Av. Vicuña Mackenna 4860, Macul, Santiago, Chile, cescauri@ing.puc.cl, http://www.ing.puc.cl/

Keywords: Turbulent Flows, Coherent Structures, Sediment Transport, Computational Fluid Dynamics.

Abstract. Large-scale unsteady coherent structures emerging from flow instabilities constitute important mechanisms of initiation of motion and sediment transport in engineering and geophysical applications. Numerical simulations of these flows are particularly challenging, especially if the objective is to capture the dynamic features of the flow at high-Reynolds numbers in complex geometries. To investigate the large-scale vortical structures that arise as a result of pressure gradients imparted on the flow by local streamline curvature or embedded solid obstacles, we carry out detached eddy simulations (DES), which successfully resolve the complex dynamics of the turbulent horseshoe vortex system around surface-mounted obstacles, and Görtler vortices in concave sediment beds. These simulations show that the numerical methods reproduce with very good accuracy all the experimental observations of mean flow quantities and turbulence statistics. Motivated by the results obtained for these flows we develop Lagrangian and Eulerian sediment transport models, which are capable of reproducing the complex dynamics of particles observed in experiments, such as intermittent bed-load transport near the threshold of motion, and the development and evolution of bedforms in fine sand.

1 INTRODUCTION

Turbulent flows in natural aquatic environments occur in arbitrary geometrical configurations, they are highly three-dimensional and characterized by a wide range vortical scales that dominate the sediment transport and erosion processes. Large-scale energetic coherent structures in these flows usually arise as a result of pressure gradients produced by embedded solid obstacles or by instabilities induced by local streamline curvature. Multiple experiments have demonstrated that the dynamics of these coherent structures can increase locally the stresses on mobile beds, initiating and enhancing considerably sediment transport rates (e.g. Dargahi, 1989, 1990; Hopfinger et al., 2004; Albayrak et al., 2008).

The complexity of flows controlled by unsteady coherent-structures in geophysical and engineering applications poses a great challenge to advanced high-resolution numerical models. Quantitatively accurate simulations can improve the engineering analysis, by providing a better understanding of the interactions between the turbulent flow and sediment transport processes in realistic conditions. The simulation of these flows are further complicated since traditional Unsteady Reynolds-averaged Navier-Stokes (URANS) turbulence models cannot reproduce the dynamics of these large-scale vortical structures in high-Reynolds number flows. In this investigation, we develop a comprehensive computational fluid dynamics model to simulate the 3D unsteady flow, bed-load transport, and localized erosion produced by large-scale unsteady coherent structures. To resolve the complex dynamics of coherent structures in turbulent flows, we carry out detached-eddy simulations (DES) (Spalart et al., 1997; Spalart, 2009), which can capture the dynamics of coherent structures in high-Reynolds number turbulent flows with moderate computational resources. We employ this model to study the horseshoe vortex system that develops in front of wall-mounted obstacles (Devenport and Simpson, 1990), and has a direct effect on sediment transport and erosion in clear-water scour conditions (Dargahi, 1990). We also investigate the development of coherent structures that arise by a centrifugal instability in a scoured concave sediment bed, to capture the increase on the shear-stress and the variations of turbulence statistics in the flow (Albayrak et al., 2008). The model allows an in-depth understanding of the flow dynamics, and it can reproduce the more complex features of bed-load transport and erosion in conditions near the threshold of motion, i.e. intermittency of particle transport and generation and evolution of bedforms in fine sand.

The paper is organized as follows: In section 2 we present the numerical methods employed in the simulations, the turbulence model, and the methodologies used in the discretization of the computational domains. In section 3 we explain the physical insights unveiled by our simulations of the turbulent horseshoe vortex system with coherent-structure-resolving turbulence models. The turbulent flow over a concave bed and the formation and dynamics of Görtler vortices are described in detail in section 4. Subsequently, in section 5 we develop new sediment transport models from Lagrangian and Eulerian standpoints to simulate the bed-load and erosion produced by the horseshoe vortex in conditions near the threshold of motion, including the dynamics of ripples that develop in fine sand. Conclusions and future research are outlined in section 6.

2 NUMERICAL METHODS

To simulate these turbulent flows in complex geometries we solve the three-dimensional unsteady Reynolds-averaged Navier-Stokes equations (URANS) with a dual-time stepping artificial compressibility scheme. The system of equations is integrated in pseudo-time using a pressure-based implicit preconditioner enhanced with local time stepping and V-cycle multigrid

acceleration (Sotiropoulos and Constantinescu, 1997). The governing equations are discretized using a second-order accurate finite-volume method on non-staggered computational grids, employing Chimera overset grids, as shown in Fig. 1, to adapt to the complex geometries using boundary-fitted structured meshes and cluster efficiently the nodes in regions of interest. For all the flows presented in this research, a no-slip boundary condition is applied to solid boundaries, and a symmetry boundary condition is imposed at the free surface for low-Froude number flows. For a detailed description of the computational methodologies the reader is referred to Paik et al. (2007).

Since conventional RANS models fail to capture the unsteadiness of the coherent structures that emerge from large-scale instabilities, and full wall-resolving large-eddy simulations (LES) might need large computational resources for practical Reynolds numbers, we employ the detached-eddy simulation (DES) approach which is a hybrid URANS/LES turbulence model developed by Spalart et al. (1997) (see also Spalart, 2009). In this investigation we have implemented the standard DES approach (Spalart et al., 1997), and a modification of the model to control the transition between the URANS and LES modes near the wall to prevent the early separation in flows past surface-mounted obstacles (Paik et al., 2007). Additionally, an Arbitrary Lagrangian-Eulerian (ALE) methodology for moving grids is incorporated into the model (Ahn and Kallinderis, 2006), to consider the moving boundary effects and couple the bed-flow interactions in simulations of scour.

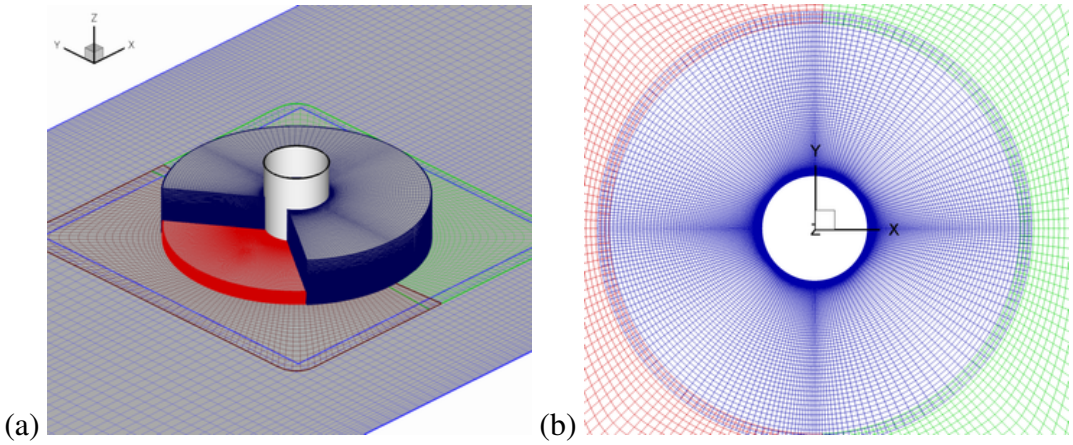

Figure 1: Computational grids for the flow past a surface-mounted cylinder (Escauriaza and Sotiropoulos, 2010b). (a) Overset grid layout with 7.2 million grid nodes, 80% around the cylinder. (b) Top view of the coarse grid with 3.0 million nodes used in the flow and sediment transport simulations of Escauriaza and Sotiropoulos (2010b,a).

3 THE TURBULENT HORSESHOE VORTEX SYSTEM

When a turbulent boundary-layer encounters a surface-mounted obstacle, the flow is dominated by the dynamically rich turbulent horseshoe vortex (THV) system around the body. In their pioneering work, Devenport and Simpson (1990) studied in detail the structure of this vortex at $Re = 1.15 \times 10^5$ in the vicinity of the leading edge of a cylindrical wing and described its dynamics by analyzing their experimental measurements at the symmetry plane in front of the obstacle. Their results showed that the THV is characterized by low-frequency oscillations that produce bimodal probability-density functions (pdfs) of velocity close to the wall. They found two separable dynamic states corresponding to the *backflow mode*, in which the return flow of the THV generates a wall jet that penetrates upstream of the obstacle, and the *zero-flow*

mode that occurs when the near-wall flow is ejected vertically upwards. The aperiodic interplay between these basic flow states produces high turbulent stresses in the junction region that are at least one order of magnitude larger than in the approaching turbulent boundary layer.

Dargahi (1989, 1990) carried out similar experiments for the flow past a vertical cylinder (diameter $D = 0.15$ m) mounted on a rectangular channel for different Reynolds numbers, and measured the THV characteristics for flat and mobile beds in fine sand with median sediment diameter $d_{50} = 0.36$ mm. The detailed analysis for $Re = 39,000$, showed that the THV consisted of a complex sequence of vortex formation and merging, with two major prevalent vortices in front of the cylinder. Turbulence statistics and oscillation frequencies were estimated between 0.1 and 2.0 Hz, with values of turbulence intensity one order of magnitude larger at the vortex location.

Numerical simulations of these flows were carried out by Paik et al. (2007) and Escauriaza and Sotiropoulos (2010b). Paik et al. (2007) performed DES of Devenport and Simpson's flow, showing that the model described in section 2 can reproduce the experimental observations by resolving practically all the significant scales of motion of the THV system, including the bimodal pdfs of velocity fluctuations and the pocket of large turbulence kinetic energy at the junction region. Additionally, the 3D analysis of the coherent structures demonstrated that the interplay between the backflow and zero-flow modes was a consequence of the development of small-scale hairpin vortices that destroyed the main THV and produced strong ejections of wall fluid, increasing the shear-stress at the wall. The details of the mechanism that produces this instability of the THV were discussed extensively in Paik et al. (2007). The growth of hairpin vortices showed to be the result of a centrifugal instability of the flow that originates at the outer turn of the THV between the vortex and the wall. For the first time the unsteady three-dimensional dynamics of the horseshoe vortex system was linked to the mechanisms that drive the quasi-periodic interplay between the backflow and zero-flow mode at the symmetry plane.

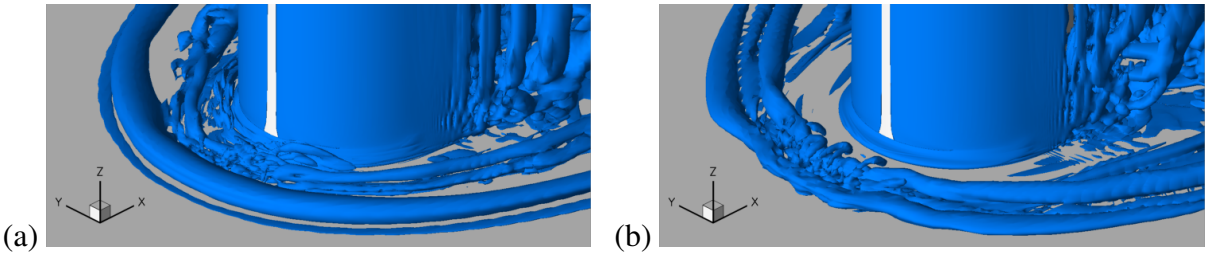

Figure 2: Instantaneous coherent structures visualized with q-isosurfaces around the cylinder for $Re = 39,000$ computed by Escauriaza and Sotiropoulos (2010b). The incoming flow is oriented in the X direction. (a) The THV system is formed by two prevalent structures. (b) Before merging occurs, the hairpin instability develops, producing eruption events in a quasi-periodic manner.

Escauriaza and Sotiropoulos (2010b) performed simulations of the flow studied by Dargahi (1989) at $Re = 39,000$, capturing all the relevant time-averaged and turbulence statistics of the flow observed in Dargahi's experiments. The instantaneous vortical structures around the cylinder, visualized with q-isosurfaces as shown in Fig. 2, reveal two large necklace-like structures wrapping around the cylinder. These structures of the THV experience a complex quasi-periodic interaction characterized by merging events and the development of hairpin vortices, following the same processes unveiled by Paik et al. (2007). Histograms of velocity fluctuations showed also to be bimodal, which is consistent with THV characteristics observed for the first time by Devenport and Simpson (1990) in the wall-mounted wing.

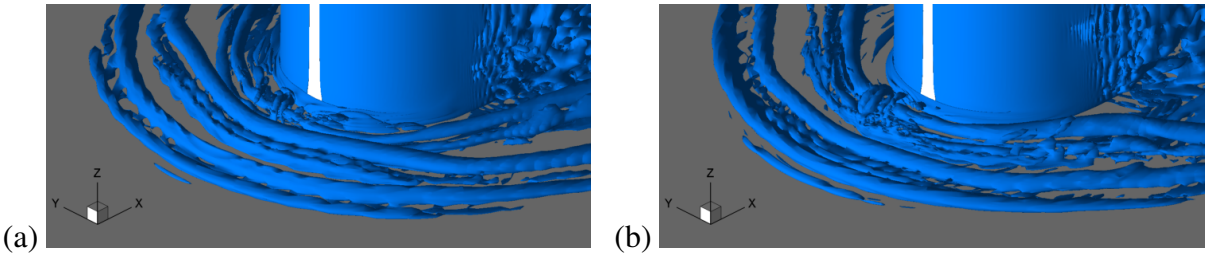

Figure 3: Instantaneous coherent structures visualized with q-isosurfaces around the cylinder for $Re = 20,000$ (Escauriaza and Sotiropoulos, 2010b). The incoming flow is oriented in the X direction. (a) The THV system is formed by up to five vortices. (b) The flow is seemingly periodic and the instability is considerably weaker compared to higher-Re cases.

Escauriaza and Sotiropoulos (2010b) also investigated the effect of the Reynolds number on the dynamics of the THV system, comparing the statistics of the experimental results of Devenport and Simpson (1990) and Dargahi (1989) with the results obtained from numerical simulations of the cylinder at $Re = 20,000$ and $Re = 39,000$. The instantaneous flow fields for low-Re show that the flow separates earlier, and that the THV is formed by a larger number of vortices that are more organized and shed in a nearly periodic manner, as depicted in the sequence of instantaneous q-isosurfaces shown in Fig. 3 (Escauriaza and Sotiropoulos, 2010b). It is important to point out that in low Reynolds number flows our simulations suggest that the eruptions of wall vorticity and hairpin instability are weaker, producing shear-stress pockets of smaller magnitude compared to high-Re cases. This variation of the THV dynamics with Reynolds number has significant consequences on the variability of the bed shear-stresses at the junction, as shown in Fig. 4. The Reynolds number effects can be clearly observed in the distribution of the standard deviation of shear-velocity u_τ at the bed. This information might be critical to understand the dynamics of sediment transport around surface-mounted obstacles and develop models to predict erosion in non-equilibrium conditions driven by the large-scale coherent structures of the flow.

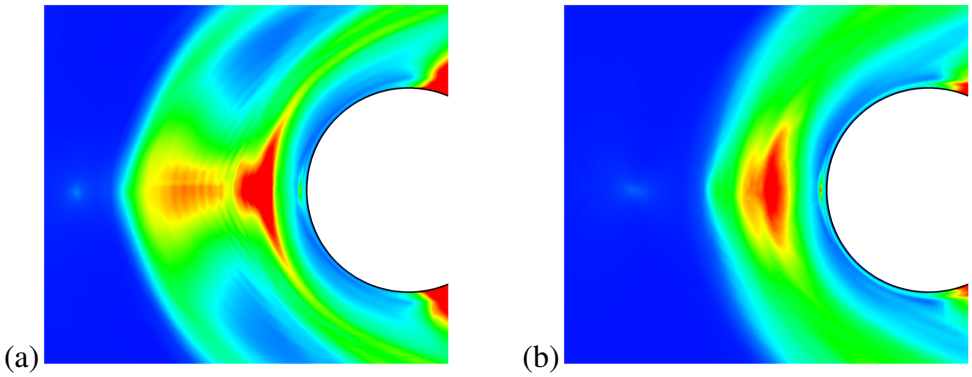

Figure 4: Non-dimensional standard deviation or root-mean square (rms) of fluctuating friction velocity u_τ shows the effect of the Reynolds number on the distribution of turbulent stresses at the bed. (a) rms distribution of u_τ for $Re = 20,000$. (b) rms distribution of u_τ for $Re = 39,000$.

4 GÖRTLER VORTICES IN CONCAVE BEDS

Hopfinger et al. (2004) and Albayrak et al. (2008) studied experimentally the scour produced by a wall-jet downstream of a sluice gate in a rectangular channel in a mobile bed with $d_{50} = 2$ mm, as shown in Fig. 5. They observed that the development of a concave bed surface due to

initial scour triggered a centrifugal instability, producing counter-rotating streamwise pairs of Görtler vortices inside the scour hole. These vortices play a significant role in the continuous development of scour as they generate high turbulent stresses and increase considerably the total sediment flux. Albayrak et al. (2008) performed statistical analyses of velocity measured with a 3D acoustic profiler on flat and concave walls, and determined the influence of Görtler vortices on Reynolds stresses.

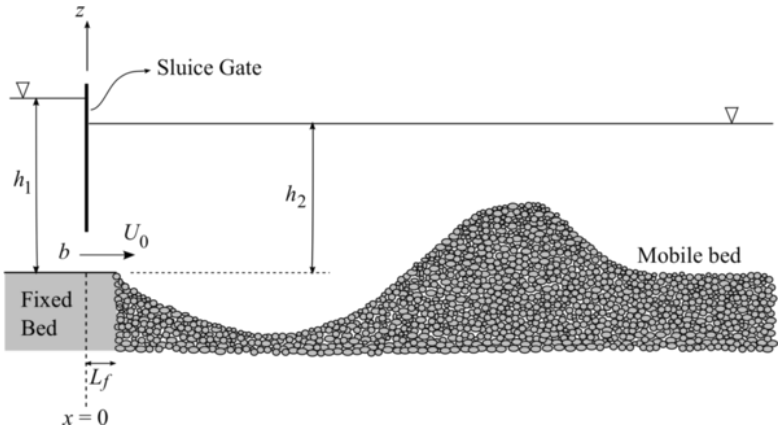

Figure 5: Sketch of the experimental configuration of the investigations of Hopfinger et al. (2004) and Albayrak et al. (2008). The Reynolds number of the flow is $Re = 156,200$ based on the velocity below the gate and the water depth in the downstream section of the channel, h_2.

We perform DES using the method described in section 2, with a mesh with 9.7 million grid nodes in the sand-bedded section of the channel to study the dynamics of Görtler vortices and their effects on the near-bed flowfield and shear-stresses. The instantaneous q-isosurfaces in the concave bed, and a vertical plane with contours of streamwise vorticity in Fig. 6 show the emergence the Görtler vortices downstream of the maximum depth inside the scour hole, coinciding with the qualitative observations of Hopfinger et al. (2004). Fig. 6(a) shows an instantaneous snapshot of q-isosurfaces colored by streamwise vorticity in which we can identify at least 5 pairs of counter-rotating vortices in the bed, formed after the flow reattaches. A zoomed area in a vertical plane across a pair of Görtler vortices is shown in Fig. 6(b). Instantaneous streamlines show clearly the formation of the vortex pair and the wall interaction.

It is important to point out that these vortices appear without imposing an unsteady pseudo-turbulent inflow condition, as the centrifugal instability is naturally excited by the resolved flowfield inside the scoured region. The upstream flow is also dominated by the shear-layer produced by the wall-jet coming from the sluice gate, which exhibits smaller time-scales compared to the Görtler vortices that appear intermittently above the bed and seem to be dominated by lower-frequencies.

Fig. 7(a) shows an instantaneous image of the shear velocity at the bed. Pockets with high values of u_τ correspond to the positions of the streamwise-oriented vortices, while lower values are located in between them. The spatial variation of shear-stress generated by the Görtler vortices is also responsible for the emergence of bedforms in the mobile bed experiments, and identified as sediment streaks by Hopfinger et al. (2004). Their experimental visualizations showed the appearance of streamwise oriented streaks on the mobile bed, which were identified as evident signs of the presence of Görtler vortices and their effects on bed-load transport and scouring processes. In our simulations, however, the bed is fixed and the sediment transport analysis for this flow will be carried out in a future investigation.

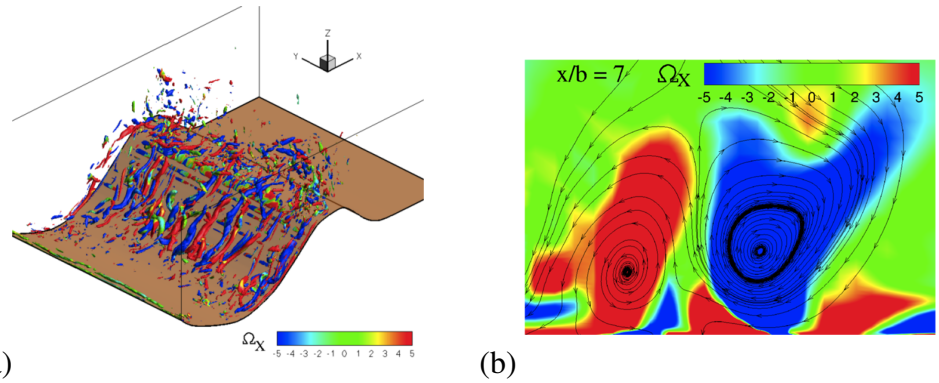

(a) (b)

Figure 6: Instantaneous flowfield in the flow downstream of a sluice gate. (a) q-isosurfaces colored by streamwise vorticity showing the emergence of Görtler vortices inside the scour hole. (b) Zoom of a cross-stream vertical plane showing contours of streamwise vorticity that depict pairs of counter-rotating vortices.

The simulated flowfield in the concave section of the channel can capture most of the turbulent stresses observed in the experiments of Albayrak et al. (2008). Fig. 7(b) shows a comparison of the non-dimensional Reynolds-stress profiles measured in the laboratory with the results of our simulations computed with the resolved flow. The model not only reproduces the location of the stress peaks in the vertical direction but also their magnitude, indicating that the model resolves most of the near-bed turbulence. The resolved flow also reproduces the upwash and downwash events produced by the Görtler vortices reported by Albayrak et al. (2008) (not shown herein), which show similar time-scales compared to the experimental measurements.

In the next section we develop Lagrangian and Eulerian sediment transport models that can utilize the resolved flowfield to predict bed-load transport and erosion driven by the large-scale coherent structures in high-Re turbulent flows. We apply these models to the flow past the surface-mounted cylinder as an example to examine their capabilities and quantitative results.

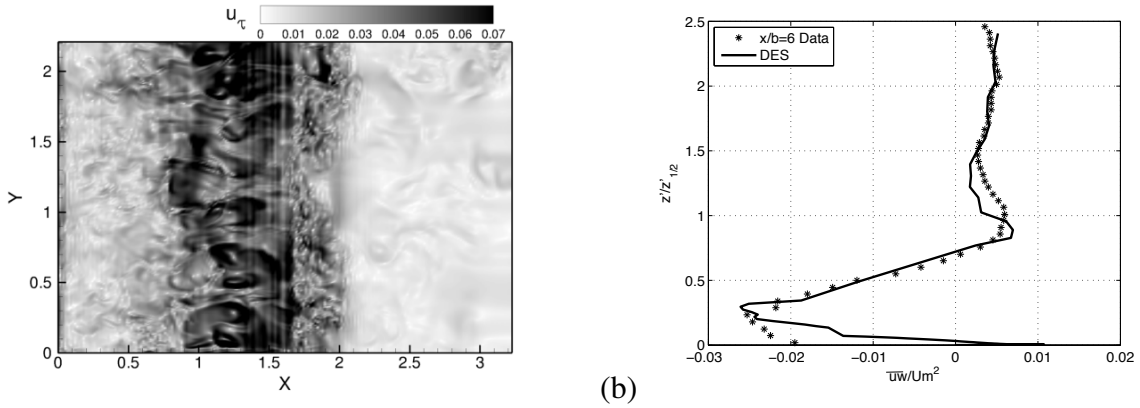

(a) (b)

Figure 7: Results from DES obtained for the flow studied by Albayrak et al. (2008). (a) Instantaneous contours of shear-velocity at the bed show pockets of high stresses at the locations of the pairs of Görtler vortices. (b) The resolved flow reproduces the Reynolds stresses measured in the experiments of Albayrak et al. (2008).

5 LAGRANGIAN AND EULERIAN SEDIMENT TRANSPORT MODELS

To investigate the direct effect of the unsteady coherent structures on the initiation of motion and particle transport, we develop a Lagrangian model to perform one-way coupling simulations of individual sediment grains for the flow studied by Dargahi (1989), since unresolved scales

do not affect the initiation of motion and particle transport of small sand grains under clear-water scour conditions. We integrate the trajectory and momentum equations for each particle, considering drag, gravity, lift, added mass, pressure and viscous forces. Therefore, the non-dimensionalized momentum equation can be written in tensor notation as:

$$\frac{dv_i}{dt} = \frac{1}{(SG + C_m)} \left[\frac{1}{St} v_{ri} - \frac{\delta_{i3}}{Fr^2} + C_L(\epsilon_{ijk} v_{rj} \omega_k) + (1 + C_m) \frac{Du_i}{Dt} \right] \tag{1}$$

where v_i is the particle velocity, ω_i is the flow vorticity, and v_{ri} the relative particle velocity with respect to the flow velocity u_i. Other dimensionless parameters appear on Eq. (1), the specific gravity of the sediment, $SG = 2.65$, the Stokes number, which is a function of the non-dimensional particle diameter ($d = d_{50}/D$), the relative velocity magnitude, and the drag coefficient C_D:

$$St = \frac{4}{3} \frac{d}{C_D \left| \mathbf{v_r} \right|} \tag{2}$$

The Froude number, Fr, defines the magnitude of the gravitational force, and the lift and added mass forces depend on the coefficients, C_L and C_m respectively. Additionally, a collision algorithm is implemented to model the particle interaction with solid boundaries (see Escauriaza and Sotiropoulos, 2009, 2010a, for details on the Lagrangian approach).

For the simulations we perform a numerical experiment with 100,000 sediment grains located initially at the bed, in front of the cylinder, using the flowfield of the THV system for the cylinder at $Re = 39,000$ computed by Escauriaza and Sotiropoulos (2010b). Since the upstream flow cannot initiate sediment motion, particles move by the effect of the instantaneous hydrodynamic forces induced by the THV. In the vicinity of the cylinder, the magnitude of the particle stresses are near the threshold of motion, thus the bed-load transport is characterized by intermittent displacement events of varying magnitudes, agreeing with numerous experimental observations of sediment transport and inertial particles in low-stage conditions. Groups of sediment grains in the THV region move continuously, saltating or sliding on the bed, and streaks aligned with near-wall vortices are formed around the pier, as shown in Fig. 8(a). Experimental evidence of the streak formation has been documented by Kaftori et al. (1995), and identified as the effect of large-scale vortical structures close to the wall that can generate enough stresses to move the particles, but cannot entrain them. The investigation of Escauriaza and Sotiropoulos (2010a) revealed that the streak particles remain in regions of relatively low shear stress, behind the main THV structures, and sediment ejections usually coincide with localized events where these zones narrow. The interaction of the vortices with the wall is therefore responsible for entrainment of particles, increasing the instantaneous forces and displacing sediment grains downstream. Escauriaza and Sotiropoulos (2010a) also showed that the sediment flux is represented by the fractal curve known as the devil's staircase, as shown in Fig. 8(b). Intermittent transport is characterized by the multifractal spectrum of the sediment flux, when statistics of transport event magnitudes are analyzed (Escauriaza and Sotiropoulos, 2010a). This Lagrangian approach constitutes the first model to give statistically meaningful particle transport driven by coherent structures in conditions near the threshold of motion (see Escauriaza and Sotiropoulos, 2010a, for details).

The representation of the realistic particle transport dynamics observed in the Lagrangian model simulations motivate the development of a new unsteady bed-load transport model to predict scour evolution around the cylinder, and the interaction of the bed with the THV. Most of the advanced CFD scour models, however, have employed Reynolds-averaged formulations to simulate the flowfield, and bed-load transport models calibrated for equilibrium conditions

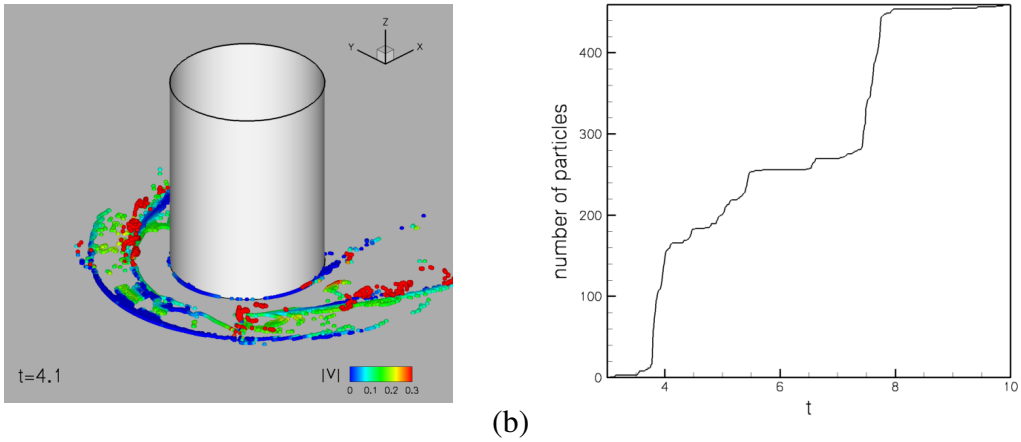

(a) (b)

Figure 8: (a) Instantaneous image of particle transport around the cylinder, particles are colored by their velocity magnitude. Image shows the two transport mechanisms by saltation and sliding, and also the streaks formed by the sediment grains around the pier. (b) Time-series of sediment flux corresponds to the fractal curve known as the Devil's staircase as verified by Escauriaza and Sotiropoulos (2010a).

in steady flows. The coherent-resolving turbulence model and the resolution of our simulations, motivate the development of a non-equilibrium bed-load transport formulation based on the particle forces considered in the Lagrangian model. We establish the sediment governing equations on the Eulerian framework, integrating directly the momentum equation averaged on the bed-load layer, assuming that the stresses due to interparticle collisions can be neglected. The instantaneous local sediment velocities parallel to the bed and integrated within the bed-load layer are found by solving the non-dimensionalized sediment momentum equation, which can be written in tensor notation as follows,

$$\frac{\partial}{\partial t}V^m + V^k \frac{\partial V^m}{\partial \xi^k} + V^k\, V^r\, \Gamma^m_{rk} = F^m \tag{3}$$

where V^m and F^m are the contravariant components of the sediment velocity and integrated forces in the $[\xi^1, \xi^2]$ coordinate system attached to the bed. The full coordinate transformation to the non-orthogonal curvilinear system in Eq. (3) include the terms Γ^m_{rk}, which are the Christoffel symbols of the second kind from the covariant derivative operator. The term F^m contains the second-order vertical integration of the particle forces that appear on the right hand side of Eq. (1) defined in the Eulerian framework, with an additional friction force to model the particle-bed interaction.

Since the instantaneous shear-stress has a close relationship with particle transport, as shown in the particle simulations of the Lagrangian model (Escauriaza and Sotiropoulos, 2010a), the instantaneous bed-load flux is computed from the particle velocity, and the bed areal concentration. At every grid node we estimate the bed areal concentration, γ, from Engelund and Fredsoe (1976) formula, which is a function of the shear-stress. The equation of the bed-load flux can thus be written in tensor notation ($j = 1, 2$), as follows:

$$q^j = \gamma\, V^j \tag{4}$$

As the ξ^3 axis of the generalized curvilinear system coincides with the vertical direction in the computational mesh, the flux components q^j in Eq. (4) correspond to the contravariant components of the bed-load flux referred to the two-dimensional coordinate system $[\xi^1, \xi^2]$,

where V^j $(j = 1, 2)$ are the contravariant components of sediment velocity in the Eulerian framework.

The mass conservation at the bed or Exner equation is solved every time-step to compute the bed elevation, and update the boundary of the computational domain with the ALE approach for moving grids:

$$\frac{\partial b}{\partial t} = \frac{-1}{(1-\lambda_p)}\left[\frac{\partial \gamma}{\partial t} + J\frac{\partial}{\partial \xi^j}\left(\frac{q^j}{J}\right)\right] \tag{5}$$

where b is the bed elevation, λ_p is the porosity that is assumed as constant and equal to 0.35, and J the Jacobian of the coordinate transformation. The critical shear stress and an avalanche algorithm incorporated into the model are computed as a function of the local slope.

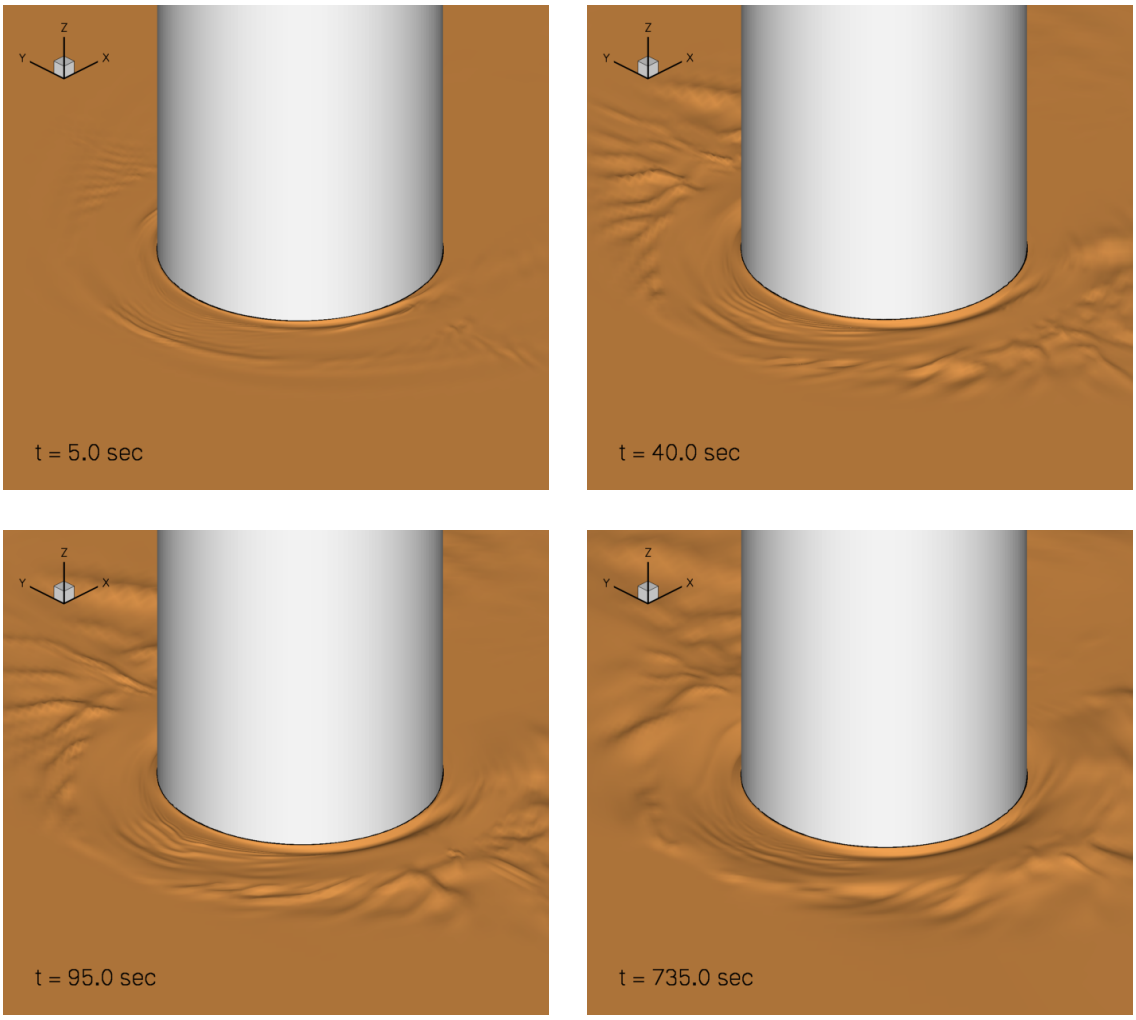

Figure 9: Instantaneous images of the bed elevation, showing the erosion process and the development of ripples around the pier.

Figure 9 shows the initial evolution of the bed by the action of the THV. The erosion is initiated at the base of the pier, and the scour hole starts to develop in front of the cylinder by the action of the unsteady coherent structures. At the symmetry plane two depressions emerge at the position of the major prevalent vortices of the THV system, which later become a single scour hole that develops at the leading edge of the pier. The scour depth time-series for the first 450 seconds, plotted in Fig. 10(a), show the rate at which the bed is eroded. The non-

equilibrium conditions determine the rapid initial scour at the two points in the THV region and the maximum scour depth on the entire bed. The maximum erosion usually occurs at the sides, on the base of the pier (approximately $\pm 45^{\circ}$ from the plane of symmetry), where the shear-stress has the largest magnitude. A particular characteristic observed at the upstream point on the symmetry plane (at the position indicated as $X/D = -0.66$) is the periodicity of the bed elevation, which occurs due to the generation of small sediment waves in the return flow of the THV that reach the transition region separating the active scour in the vicinity of the pier from the low shear-stress zone with no mobility.

Fig. 10(b) shows contours of bed elevation in a coordinate defined along the centerline of the ripples, on one side of the cylinder, to illustrate the bedform evolution in time and space. From the topography contours, we can identify the appearance of structures of different sizes, and multiple merging episodes that occur as time progresses. The bedforms are generated periodically near the symmetry plane (located at the coordinate origin $S = 0$), initially move at very high velocities but subsequently slow down as they merge to form larger structures. The ripple celerity is relatively similar to the experimental measurements of 0.1 m/s for small bed forms reported by Dargahi (1990). Large ripples that are formed by merging, however, travel slowly and become more persistent in time.

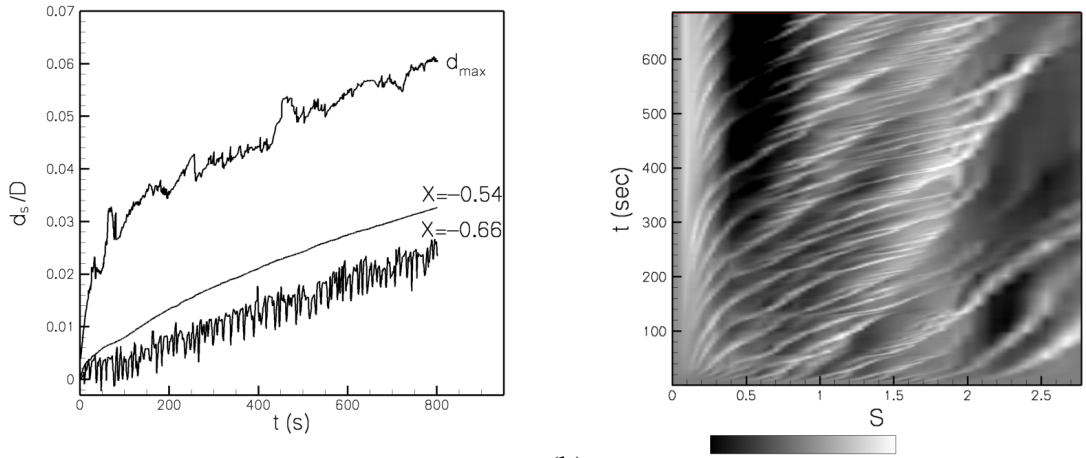

(a) (b)

Figure 10: (a) Progress of scour depth at two different points on the symmetry plane upstream of the cylinder, and maximum erosion on the bed. (b) Space-time contours of bed elevation across the ripples show the propagation of bedforms along the bed, and the merging events that produce larger more-stable ripples.

6 CONCLUSIONS

We carried out numerical simulations of turbulent flows in which large-scale coherent structures constitute the most important mechanism of sediment transport and erosion. These unsteady vortices arise by the presence of surface-mounted obstacles in the flow (Dargahi, 1989; Devenport and Simpson, 1990), or by the streamline curvature generated by complex topography of scoured beds, identified as Görtler vortices in recent experiments (Hopfinger et al., 2004; Albayrak et al., 2008).

We analyzed in detail the flow past a cylindrical pier for flat and mobile beds at Re=39,000, with the configuration studied experimentally by Dargahi (1989, 1990). The DES simulations captured the dynamic characteristics of the THV, including the frequency range of turbulent fluctuations observed in the experiments and the bimodal pdfs of velocity. A Lagrangian model

was developed to perform one-way coupling simulations of individual sediment grains, and investigate the effects of the unsteady flow on the sediment transport. The trajectory and momentum equations for each particle are computed by considering drag, gravity, lift, added mass, pressure and viscous forces. For particles initially located at repose on the bed, at the THV region, the model reproduces the intermittent transport that is commonly observed in situations near the threshold of motion. The complex interactions of the large-scale coherent structures with the wall produce regions of higher shear-stress and vertical velocity, which trigger the intermittent displacement of groups of particles. Besides these ejection events, other phenomena observed in sediment transport experiments are also reproduced, such that particle sliding, saltation, and streak formation aligned with near-bed vortices.

The same model is utilized to develop an unsteady bed-load transport model. The sediment momentum equation is integrated in an Eulerian framework, and the bed-load flux is obtained by estimating the areal concentration from an empirical relation. The Exner equation is solved every time-step, and the bed elevation is updated to incorporate the scour effects on the flowfield through an ALE approach for moving grids. The model reproduces scour in non-equilibrium conditions, and allows quantitative analyses of the initial development of scour by providing complete information of the spatial distribution and time evolution of erosion and deposition. The model can also capture the emergence and development of ripples along the legs of the THV, which were also documented on Dargahi's (1990) experiments. With the methodology presented in this investigation we can simulate bed-load transport produced by the large-scale coherent structures in clear-water scour conditions. The sediment is assumed as fine sand, and the transport diluted, such that the stresses due to collisions of particles can be ignored. For sediment transport flows with higher concentrations, the model would require a stronger coupling between the flow and the sediment, accounting for the particle forces on the URANS equations, and also consider the stresses due to interparticle collisions on the sediment dynamics. To address more general situations with suspended load, we would need to incorporate the sediment governing equations for the entire domain linked to the bed-load layer.

In summary, the model constitutes an advanced computational framework to study bed-load transport and scour in realistic conditions. The numerical results can give insights on the mechanisms of erosion, entrainment, transport dynamics, and evolution of scour in unsteady flows with complex geometries at high Reynolds numbers with deformable beds. These results show that the model can be employed in the future to guide engineering analysis and design, and identify the parameters that are relevant to characterize turbulent flows and predict sediment transport rates and erosion in non-equilibrium conditions.

7 ACKNOWLEDGEMENTS

This work has been carried out in collaboration with Dr. J. Paik, Dr. F. Sotiropoulos, and Mr. B. Rodríguez, and it has been supported by Fondecyt grant 11080032.

REFERENCES

Ahn H.T. and Kallinderis Y. Strongly coupled flow/structure interactions with a geometrically conservative ALE scheme on general hybrid meshes. *J. Comput. Phys.*, 219:671–696, 2006.

Albayrak I., Hopfinger E.J., and Lemmin U. Near-field flow structure of a confined wall jet on flat and concave rough walls. *J. Fluid Mech.*, 606:27–49, 2008.

Dargahi B. The turbulent flow field around a circular cylinder. *Exp. Fluids*, 8:1–12, 1989.

Dargahi B. Controlling mechanism of local scour. *J. Hydraul. Eng.*, 116:1197–1214, 1990.

Devenport W.J. and Simpson R.L. Time-dependent and time-averaged turbulence structure near the nose of a wing-body junction. *J. Fluid Mech.*, 210:23–55, 1990.

Engelund F. and Fredsoe J. A sediment transport model for straight alluvial channels. *Nordic Hydrol.*, 7:293–306, 1976.

Escauriaza C. and Sotiropoulos F. Trapping and sedimentation of inertial particles in three-dimensional flows in a cylindrical container with exactly counter-rotating lids. *J. Fluid Mech.*, 641:169–193, 2009.

Escauriaza C. and Sotiropoulos F. Lagrangian model of bed-load transport in turbulent junction flows. *accepted for publication in J. Fluid Mech.*, 2010a.

Escauriaza C. and Sotiropoulos F. Reynolds number effects on the coherent dynamics of the turbulent horseshoe vortex system. *accepted for publication in Flow Turbul. Combust.*, 2010b.

Hopfinger E.J., Kurniawan A., Graf W.H., and Lemmin U. Sediment erosion by Görtler vortices: The scour-hole problem. *J. Fluid Mech.*, 520:327–342, 2004.

Kaftori D., Hetsroni G., and Banerjee S. Particle behavior in the turbulent boundary layer: I. Motion, deposition, and entrainment. *Phys. Fluids*, 7:1095–1106, 1995.

Paik J., Escauriaza C., and Sotiropoulos F. On the bimodal dynamics of the turbulent horseshoe vortex system in a wing-body junction. *Phys. Fluids*, 19:045107, 2007.

Sotiropoulos F. and Constantinescu G. Pressure-based residual smoothing operators for multi-stage pseudocompressibility algorithms. *J. Comput. Phys.*, 133:129–145, 1997.

Spalart P.R. Detached-eddy simulation. *Annu. Rev. Fluid Mech.*, 41:181–202, 2009.

Spalart P.R., Jou W.H., Strelets M., and Allmaras S.R. Comments on the feasibility of LES for wings and on a hybrid RANS/LES approach. In C. Liu and Z. Liu, editors, *Advances in DNS/LES*. Greyden Press, Columbus OH, 1997.